White Rose Research Online

eprints@whiterose.ac.uk
https://eprints.whiterose.ac.uk
Universities of Leeds, Sheffield and York

Deposited via The University of Sheffield.

White Rose Research Online URL for this paper:
https://eprints.whiterose.ac.uk/id/eprint/194933/

Version: Accepted Version

**Article:**
Li, P., Susmel, L., Jiang, W. et al. (2023) The porosity distribution of nickel-base single-crystal superalloy DD5 and its fatigue life property. Fatigue and Fracture of Engineering Materials and Structures, 46 (4). pp. 1545-1553. ISSN: 8756-758X

https://doi.org/10.1111/ffe.13947

This is the peer reviewed version of the following article: Li, P, Susmel, L, Jiang, W, Yin, H. The porosity distribution of nickel-base single-crystal superalloy DD5 and its fatigue life property. Fatigue Fract Eng Mater Struct. 2023, which has been published in final form at https://doi.org/10.1111/ffe.13947. This article may be used for non-commercial purposes in accordance with Wiley Terms and Conditions for Use of Self-Archived Versions. This article may not be enhanced, enriched or otherwise transformed into a derivative work, without express permission from Wiley or by statutory rights under applicable legislation. Copyright notices must not be removed, obscured or modified. The article must be linked to Wiley's version of record on Wiley Online Library and any embedding, framing or otherwise making available the article or pages thereof by third parties from platforms, services and websites other than Wiley Online Library must be prohibited.

**Reuse**
Items deposited in White Rose Research Online are protected by copyright, with all rights reserved unless indicated otherwise. They may be downloaded and/or printed for private study, or other acts as permitted by national copyright laws. The publisher or other rights holders may allow further reproduction and re-use of the full text version. This is indicated by the licence information on the White Rose Research Online record for the item.

**Takedown**
If you consider content in White Rose Research Online to be in breach of UK law, please notify us by emailing eprints@whiterose.ac.uk including the URL of the record and the reason for the withdrawal request.

UNIVERSITY OF LEEDS
University of Sheffield
UNIVERSITY of York

# The porosity distribution of Nickel-base single crystal superalloy DD5 and its fatigue life property

Piao Li[1,2*] Luca Susmel[1] Wen Jiang[3,4] Haibiao Yin [2]

([1]Department of Civil and Structural Engineering, The University of Sheffield, Sheffield S1 3JD, UK)

([2]College of Aerospace Engineering, Nanjing University of Aeronautics and Astronautics, Nanjing 210016, China)

([3]Nanjing Engineering Institute of Aircraft Systems, AVIC, Nanjing 211106, China)

([4]Aviation Key Laboratory of Science and Technology on Aero Electromechanical System Integration, Nanjing 211106, China)

**Abstract:** The porosity of nickel-base single crystals (NBSX) is still an unavoidable casting problem that has a significant influence on the fatigue life of NBSXs. In order to quantify the porosity effect, a porosity-distribution-related life prediction method is proposed in this paper. The porosity size in a NBSX was measured and the size distribution was regressed. The results show that the porosity size which is characterized by Feret diameter follows a modified logarithmic normal distribution. The relation among the applied stress, porosity size and lifetime is expressed by using the proposed method. The disperse band of S-N curve is investigated based on the probability distribution of the porosity size. The results show that the predicted S-N curve agrees well with the experimental data.

**KYEWORDS:** Nickel-base single crystal, porosity, fatigue, S-N curve

* Corresponding author. E-mail address: lipiao@nuaa.edu.cn

## 1. INTRODUCTION

Niciel-base single crystal (NBSX) superalloy is the main material of aeroengine turbine blades. Due to the elimination of the grain boundaries where cracks are prone to initiate, the mechanical properties of NBSX have been significantly improved compared to polycrystalline materials. This feature makes NBSXs a preferential solution for the manufacturing of turbine blades. Due to the working condition of high-temperature, high-pressure and complex load, turbine blades suffer from mechanical failure problems, of which fatigue is a predominant failure mode.

The diffuse pores remain an unavoidable problem in the casting of directionally solidified NBSXs.[1] The effect of porosities on the fatigue performance of NBSX cannot be neglected, which has been widely investigated ln the last three decades. [2-5] The fatigue performance of NBSX is one of the focuses of these previous investigations. Bouchenot et al.[6] proposed an analytical stress-strain hysteresis model based on thermomechanical fatigue mechanisms, which can enhance the ability of LCF life estimation. Rai et al. [7] investigated the dislocation and cyclic plastic deformation behaviour of a nickel base superalloy through extensive scanning electron microscope (SEM) and transmission electron microscope (TEM) examinations. The low cycle fatigue behavior of NBSX at elevated temperature has been widely investigated experimentally.[8-15] Ravi Chandran [16, 17] presented an S-N curve model employing the Gumbel distribution. Vacchieri et al. [18] used the safe life approach to estimate the fatigue life of a gas turbine first-stage blade. The Theory of Critical Distances was used to predict the fatigue life in notched single crystal superalloy components. [19, 20] Yuan et al. [21] concluded that the lifetime of NBSX CMSX-4 under thermal mechanical cyclic loading is significantly affected by the temperature gradient and then proposed a modified model to consider the temperature gradient effect and the thermal-mechanical phase angle. Other factors influencing the fatigue performance of NBSX have also been experimentally and numerically studied, such as the secondary crystal orientation [22-24], mean stress [25], tension-torsion multiaxial loading [26-28], size-effect [29, 30], etc. Porosity size and its distribution are the key factor that affects the fatigue life of NBSXs. Rémy et al.[31] proposed an engineering damage model to describe the micro-crack growth from

pores based on a process zone concept. Musinski et al. [32] presented a formulation that links the microstructure heterogeneity (grain size distribution) to size effect and fatigue scatter in notched polycrystalline Ni-base superalloy IN100 specimens. Microstructure-based fatigue life models have been considered in detail by many researchers. [33-38] However, just a few investigations have been conducted to quantify the existing links between porosity distribution and fatigue lifetime of NBSXs.

Murakami's theory has laid the foundations for the research on the fatigue behavior of metallic materials that contain small defects and non-metallic inclusions. [39] Based on the available knowledge [40-43], this paper focuses on the S-N curve dispersion of NBSX DD5 caused by pore size distribution. A Porosity-distribution-related life prediction model is proposed, and the test results are used for validation.

## 2. POROSITY-DISTRIBUTION-RELATED LIFE PREDICTION METHOD OF NBSX

### 2.1 Material and specimen

The test material was the second generation nickel base single crystal superalloy DD5 made in China. [43] Compared to the first generation, the high-temperature resistance of DD5 has been further enchanced thanks to the introduction of refractory element Re (3%). The nominal composition of the alloy is given in Table 1. The tensile properties in the [001] direction at 980 °C and the engineering elastic constants in the [001] direction at 1000 °C are reported in Table 2.

TABLE 1 The nominal composition of DD5(wt%)

| Cr | Co | Mo | W | Ta | Re | Hf | Al | C | Ni |
|---|---|---|---|---|---|---|---|---|---|
| 7 | 8 | 2 | 5 | 7 | 3 | 0.2 | 6.2 | 0.05 | Balance |

TABLE 2 The mechanical properties of DD5 (in [001] direction)

| Elastic modulus E/GPa | Poisson's ratio $\mu$ | Shear modulus G/GPa | Yield strength $\sigma_{0.2}$/MPa | Ultimate strength $\sigma_b$/MPa |
|---|---|---|---|---|
| 95.34 | 0.416 | 89.7 | 792 | 850 |

The single crystal test bars were produced by using the spiral crystal selection method in a high gradient vacuum induction furnace. The designed axis orientation of the bars is [001], and the orientation deviation is controlled to be within 15°. To obtain specially introduced pores with a certain pore size in the test bars, an alumina ceramics filter with different mesh densities was used in the casting to control the gas content. Two groups of test bars with different porosity size distribution were finally obtained, and further processed into the shape of test pieces, as shown in Figure 1.

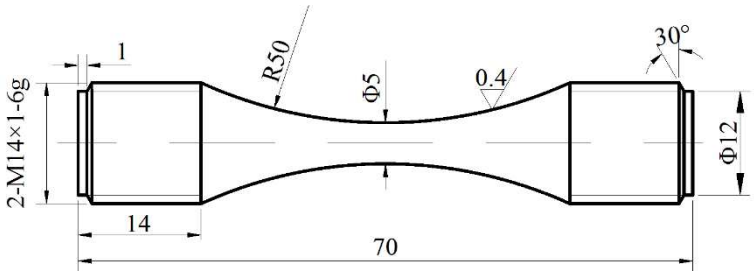


FIGURE 1 The configuration of test piece (unit: mm)

**2.2 Porosity characterization**

In order to obtain the porosity size distribution of the NBSX specimens being tested, metallographic observations were carried out on 12 randomly selected view fields of the two groups of samples. The samples were cut along the axial [001] direction of the test piece, and careful mirror polishing was applied to the nominal (001) plane of the samples by the order of using 600#, 800#, 1000#, 1200#, 1500#, 2000#, 3000#, and 5000# sandpaper for preliminary grinding, followed by 5, 3.5, and 0.5 μm diamond polishing paste to remove the surface small scratches. Finally the 0.05 and 0.02 micron silica fine polishing liquid was used for final finish. The mirror-polished samples were placed under the optical microscope VHX-1000 3-DVM for metallographic photography.

A representative view field is shown in Figure 2(a). It can be seen that the pores are clearly distributed on the sample surface. In order to eliminate the influence of low-qualified image noise, the defects smaller than 10 pixels (which is equal to an effective diameter of ~5 μm ) were not taken into account.

It can be seen from Figure 2(a) that the shape of the pores is not regular. In order

to quantitatively describe the size of pores, it was necessary to define a uniform rule. Both Murakami's parameter $\sqrt{area}$ [44] and Feret's diameter $\phi_{surr}$ [45, 46] are widely used in situations of practical interest. Murakami's parameter is defined as the square root of the projected area of the defect in the direction perpendicular to the principal stress. Feret's diameter is defined as the diameter of the circumscribed circle of the defect, as shown in Figure 2(b). Since Feret's diameter has a better accuracy and reliability in quantifying the size of defects with complex shapes, [45, 46] in what follows it will be used to characterize the pore size.

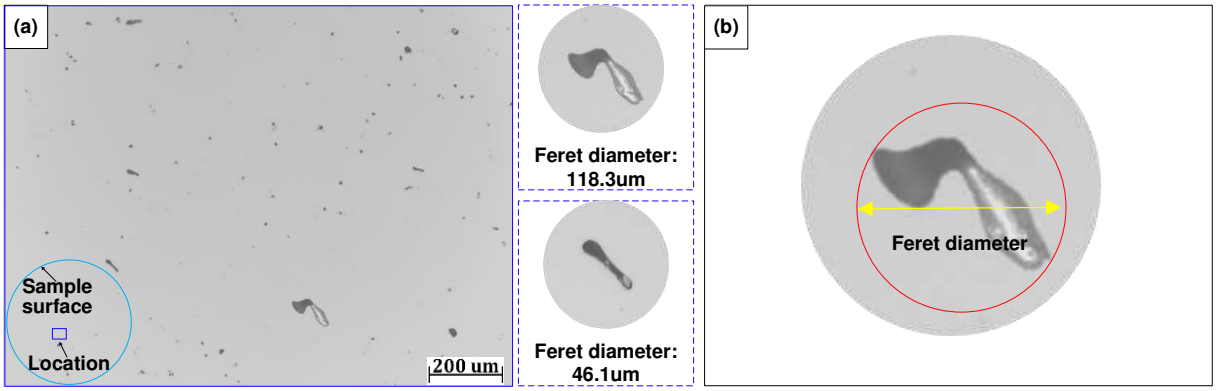


FIGURE 2 The metallographic observation: (a) a representative view field, (b) the definition of feret diameter

The final measurement results of the size distribution of the two groups of samples are shown in Figure 3. It can be seen that the size distribution of NBSX can be well described via a log-norm distribution. For both groups, about 85% of the pores were seen to have size in the range 10-20 μm. In the tail distribution part, the second group was characterised by larger pores, which means that the large pores in the second group were on average larger than those in the first group. The observed largest pore in the first group had size equal to 90.1 μm, whereas the observed largest pore in the second group to 138.4 μm. Thus the first group was named Group S and the second named Group L thereinafter.

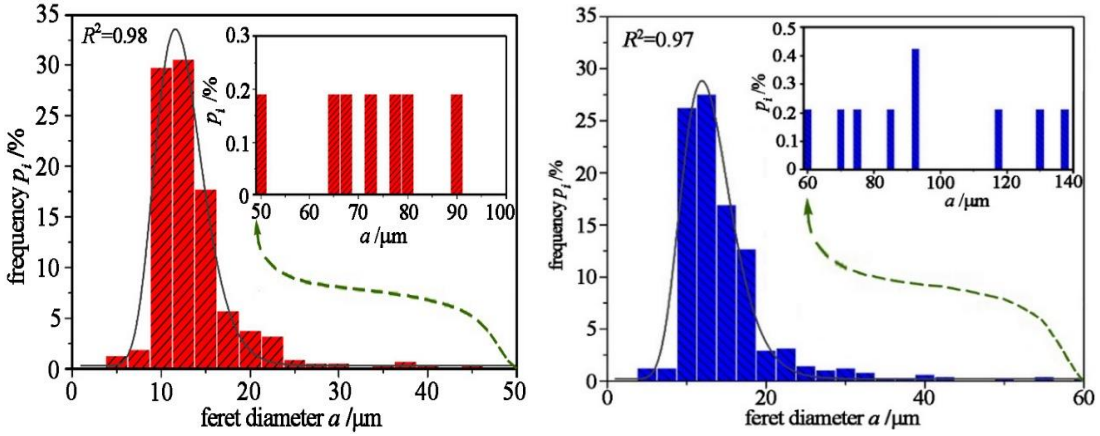


(a) Group S (b) Group L

FIGURE 3 Pore size distribution of NBSX: (a) Group S; (b) Group L

### 2.3 S-N curve prediction

As discussed above, Feret's diameter, $a$, was employed to mearsue the size of a porosity and follows a modified logarithmic normal distribution that can be described as:

$$f(a) = f_0 + \frac{A}{\sqrt{2\pi}\sigma_a d}\exp\left(-\frac{(\ln a - \mu_a)^2}{2\sigma_a^2}\right) \tag{1}$$

For the two groups of samples, the values of the parameters in Equation 1 are listed in Table 3.

TABLE 3 Distribution parameters

| | $f_0$ | $A$ | $\mu_a$ | $\sigma_a$ |
|---|---|---|---|---|
| Group S | 0.00132 | 0.88168 | 2.50 | 0.22 |
| Group L | 0.00076 | 0.90264 | 2.54 | 0.25 |

According to Murakami's theory, when the defect is small, it can be treated as a crack. [39]

Accroding to Paris's law, the growth of crack can be modelled and quantified as:

$$\frac{da}{dN_f} = C\left[S\sqrt{\pi a(t)}\right]^M = Q\left[a(t)\right]^b \tag{2}$$

where $Q$ is a parameter which is related to loading $S$, $b$ is a material constant which is close to but greater than 1, $a$ is the equivalent crack length, and $N_f$ is the number of

fatigue cycles. After integration of Equation 2, it is straightforward to obtain:

$$N_{\mathrm{f}} = \frac{1}{Q(1-b)}\left(\frac{1}{a_{\mathrm{c}}^{b-1}} - \frac{1}{a_0^{b-1}}\right) \tag{3}$$

where $a_0$ is the initial equivalent crack diameter, and $a_{\mathrm{c}}$ is the critical fracture crack length. Since $b \geq 1$, and $a_{\mathrm{c}} >> a_0$, Equation 3 can be rewritten as

$$N_{\mathrm{f}} = \frac{1}{Q(b-1)} \cdot \frac{1}{a_0^{b-1}} \tag{4}$$

Considering the fatigue limit of the material ($S_{\mathrm{e}} \geq 0$) and assuming that $Q$ can be written in the following form:

$$Q = \frac{1}{C}\left(1 - \frac{S_{\mathrm{e}}}{S}\right)^{2b} \tag{5}$$

where $S$ is the applied loading, $C$ is a constant, Equation 3 can then be written as

$$N_{\mathrm{f}} = \frac{C}{\left(1 - \frac{S_{\mathrm{e}}}{S}\right)^{2b} \cdot (b-1)} \cdot \frac{1}{a_0^{b-1}} \tag{6}$$

Equation 6 is an S-N curve model which contains three parameters, $C$, $b$ and $S_{\mathrm{e}}$.

According to Murakami's theory, [44] the fatigue limit of NBSX can be obtained as:

$$S_{\mathrm{e}} = 1.43(HV + 120) / \sqrt[6]{\pi a^2} \tag{7}$$

where $HV$ is the Vickers hardness, $a$ is the equivalent crack length.

According to Equation 7, the fatigue limit is related to the hardness and the defect size of the material, since hardness is a value that can be obtained through tests, fatigue limit can be uniquely determined by the defect size. Once the defect size and its distribution are obtained, the fatigue life distribution can be deduced by combining Equation 6 and Equation 7.

## 3. FATIGUE TEST AND MODEL VERIFICATION

### 3.1 Test implementation

In order to obtain the S-N curve data of the two groups of NBSX, the high cycle

fatigue tests were designed to be carried out under four stress levels. At least three test pieces were prepared for each stress level. The material and test piece configuration have been presented in Section 2.1. The test equipment is the GBQ50-B high frequency fatigue testing machine, and the maximum loading capacity of the testing machine is ±50KN. The loading frequency is 110Hz and the test temperature is 980 °C. Before the test, the test piece was installed on the test machine through the clamp, and the thermocouple was tied to the middle of the test piece for temperature measurement. Before loading, the test piece was placed in the high-temperature furnace and slowly preheated to 980 °C. The loading was not applied until the temperature was stable and the temperature fluctuation did not exceed 3°C. The loading waveform was a sinusoidal wave and the stress ratio was set equal to 0.1.

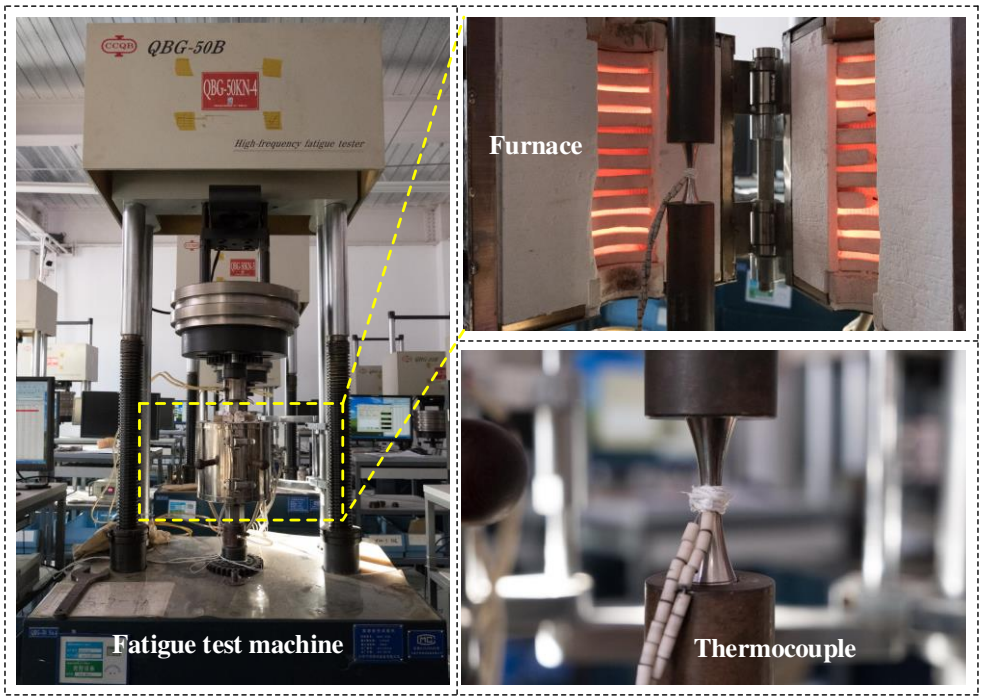


FIGURE 4 Test implementation

### 3.2 Test results and model verification

3.2.1 Group S

The test results of Group S are listed in Table 4. From this table it is straightforward to see that the fatigue life of NBSX was inversely proportional to the porosity size under a certain cyclic loading. For example, the fatigue crack of specimen S8 initiated from a

pore with 44.6 μm in size, and the fatigue life of S8 was $1.768\times10^6$cycles. While under the same stress level, the specimen S10 had a fatigue life of only $4.0\times10^4$ cycles, because the pore size of S10 was equal 334.2 μm. It can be seen from Fig.5 that the fatigue limit corresponding to $10^7$ cycles was within 480MPa~540MPa.

TABLE 4 Fatigue test results of Group S

| Specimen No. | $S_{max}$ / MPa | $N_f$ /$10^3$ | $a_0$ / μm |
|---|---|---|---|
| S1~S3 | 765 | 130 113 198 | 96.6 103.1 90.4 |
| S4~S6 | 710 | 202 343 482 | 120.5 92.7 72.6 |
| S7~S8, S10 | 640 | 701 1768 40 | 77.7 44.6 334.3 |
| S11~S12, S14~S15 | 560 | 1120 2572 475 3092 | 142.1 90.1 243.5 103.2 |
| S20, S26 | 540 | 7765 >10000 | 80.4 46.6 |
| S19, S21, S23, S25 | 520 | 11518 3,361 8077 >10000 | 42.9 105.8 82.8 72.3 |
| S16, S18, S22, S24 | 500 | 7005 14229 >10000 >10000 | 137.5 59.3 84.4 68.6 |
| S17 | 480 | >15000 | 43.4 |

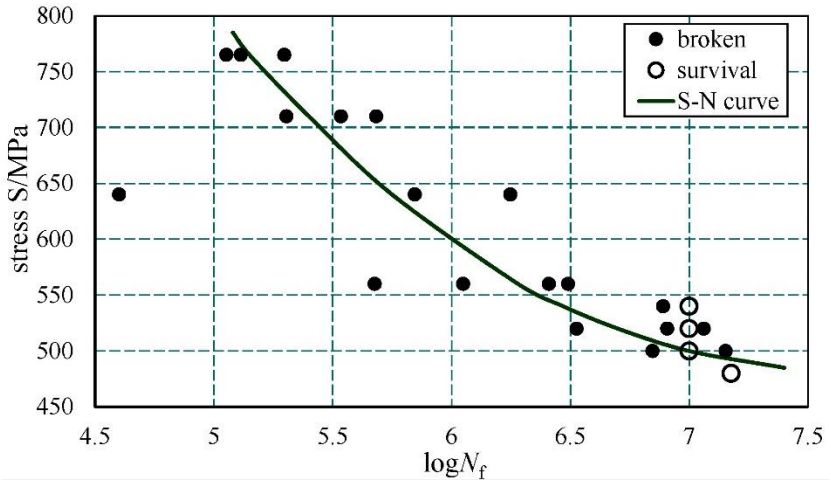


FIGURE 5 S-N curve of Ni-based single crystal superalloys at 980℃ (Group S)

The microhardness tester was adopted to measure the hardness of DD5. For each group, 12 samples were tested, and on each sample, 5 points were tested and the final hardness was taken as the average value. The results show that there is not obvious difference in the hardness of the two groups, and the Vickers hardness of Group S and Group L are separately 455.5kgf/mm$^2$ and 448.9kgf/mm$^2$.

The porosity distribution of DD5 were obtained via Equation 1. After obtaining the porosity distribution and the hardness, the fatigue limit distribution was derived from Equation 7. Table 5 lists the statistical parameters of the equivalent pore size and the calculated fatigue limit for the samples belonging to Group S.

TABLE 5 Statistical parameters of equivalent pore size $a$ and calculated fatigue limit (Group S)

| Statistical parameter | value/ μm | $S_e$/MPa |
|---|---|---|
| Average $\bar{a}$ | 15.6 | 520.6 |
| $a_{5\%}$ | 7.4 | 589.5 |
| $a_{95\%}$ | 45.9 | 434.9 |
| $a_{95\%}$ | 45.9 | 434.9 |

After obtaining the statistical parameters, the values of $C$ and $b$ in Equation 6 were obtained by using the fitting method (stress level, fatigue life and initial defect size $a_0$ are given in Table 1). By combining with the data in Table 3, the average S-N curve and its 5% and 95% boundaries were obtained, as shown in Figure 6.

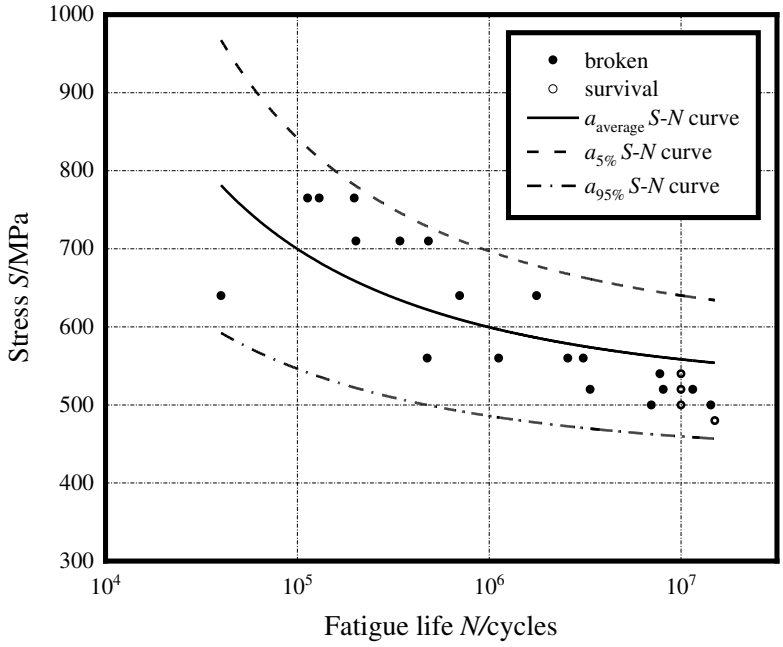


FIGURE 6 S-N curves estimated by Equation 6 and experimental data (Group S)

It can be seen from Fig.6 that all the experimental data fall into the 5% and 95% boundary, and the predicted average S-N curve well describes the actual experimental data distribution. This fully proves the validity of the proposed method.

3.2.2 Group L

The test results generated by testing the samples from Group L are listed in Table 6. The tendency of the test results of Group L is the same as that described for the specimens from Group S. For a given stress level, a test piece with a larger porosity size showed a lower fatigue life than another one containing smaller pores.

TABLE 6 Test results of Group L

| Specimen No. | $S_{max}$ / MPa | $N_f$ /$10^3$ | | | $a_0$ / μm | | |
|---|---|---|---|---|---|---|---|
| L1~L3 | 765 | 42 | 54 | 36 | 124.0 | 120.0 | 140.2 |
| L4~L6 | 710 | 151 | 174 | 116 | 108.5 | 112.7 | 118.9 |
| L7~L9 | 640 | 959 | 421 | 1168 | 134.1 | 1820. | 107.0 |
| L11~L13 | 560 | 2989 | 5342 | 3905 | 108.3 | 116.1 | 120.9 |

| Specimen No. | $S_{max}$ / MPa | $N_f$ /$10^3$ | | | | $a_0$ / μm | | | |
|---|---|---|---|---|---|---|---|---|---|
| L14, L16, L19, L21 | 490 | 8994 | 7371 | 6029 | 13204 | 102.2 | 115.6 | 127.5 | 89.7 |
| L15, L20 | 470 | 13330 | >10000 | | | 102.7 | 93.5 | | |
| L18 | 450 | >10000 | | | | 70.6 | | | |

The porosity distribution characterising Group L was again determined via Equation 1. After determining the porosity distribution and the hardness, the fatigue limit distribution was estimated from Equation 7. Table 7 lists the statistical parameters of the equivalent pore size and the calculated fatigue limit for the samples from Group L.

TABLE 7 Statistical parameters of equivalent pore size $a$ and calculated fatigue limit (Group L)

| Statistical parameter | Value/ μm | $S_e$/MPa |
|---|---|---|
| Average $\bar{a}$ | 17.1 | 512.9 |
| $a_{5\%}$ | 7.4 | 589.3 |
| $a_{95\%}$ | 55.2 | 421.7 |

Following the same method as the one used to post-process the results from the previous group, the average S-N curve and its 5% and 95% boundaries were determined also for Group L. The results are shown in Figure 7. In total 22 test pieces were in Group L and, among them, 19 test pieces were cyclically tested. The test results were compared with the predicted S-N curves, as shown in Figure 7.

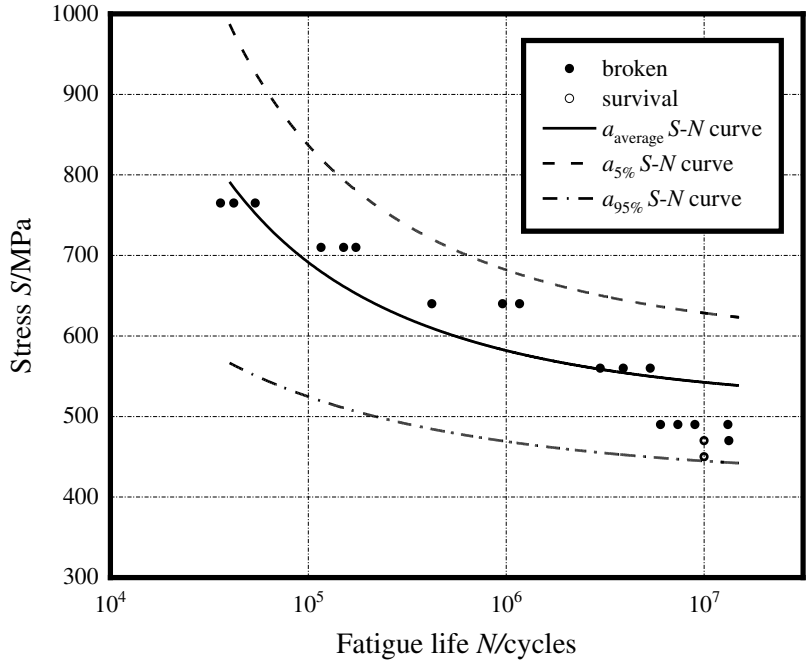


FIGURE 7 S-N curves estimated by Equation 6 and experimental data (Group L)

It can be seen that all the test data fall into the predicted 5% and 95% S-N scatter band. Most of the test data matches well the predicted average S-N curve, except that the test data in the $10^7$ cycles to failure region that slightly deviate from the average S-N curve and are closer to the 95% S-N curve. This can be explained from our previous research result: when the NBSX is loaded under a high temperature and when a long lifespan can be expected, oxidation from the specimen surface can have a synergistic effect with the porosity, with this resulting in an increase of fatigue damage. [47] However, it is possible to conclude by saying that, in general, the predicted S-N curve can well describe the distribution of the test data, which demonstrates again the validity of the proposed method.

## 4. DISCUSSION

### 4.1 Link between porosity distribution and life distribution

It can be seen from the analyses discussed in the previous sections that the fatigue lifetime is influenced by the distribution of porosity. To perform the complete analysis,

at least three fatigue test data are necessary, which makes the analysis simple and fast. Since the life distribution is almost uniquely determined by the porosity distribution, the accuracy of predicted S-N curve strongly depends on the accuracy of the porosity distribution. Besides, it is obvious that more fatigue test data can lead to a more precise S-N curve configuration.

### 4.2 Other influencing factors

When porosity is not the main reason that leads to fatigue failure, the predicted life distribution can deviate from the actual S-N curve. According to Section 3.2, for both groups the fatigue lives of the tested specimens are shorter than the predicted average fatigue life at the life interval in the $10^7$ cycles to failure region. This is the result of the synergistic effect with oxidation. In other cases, for example, under the concomitant effect of creep, corrosion or other factors, the additional damage should be taken into account carefully to avoid non-conservative estimates.

## 5. CONCLUSIONS

Diffuse porosity still remains an unavoidable problem in the casting process of directionally solidified nickel-base single crystals. The introduced largest pore can reach a size of the order of hundred microns. These pores acts as local stress concentrators, triggering the fatigue crack initiation process. In order to quantify the influence of porosity on the fatigue strength, a model is proposed in this paper to describe the stress-life behavior of nickel-base single crystals. The conclusions can be drawn as follows.

(1) The distribution of porosity size is introduced into the relation of stress and fatigue life, so that a new perspective to describe the S-N curve is established.

(2) The distribution of fatigue life strongly depends on the distribution of porosity. According to the proposed model, the S-N curve scatter band under different life probabilities can be obtained once the distribution of porosity is obtained.

(3) Under the current investigated background, when porosity is the direct cause

of fatigue failure, the predicted life distribution agrees well with the experimental life data, which demonstrates that the proposed model can well describe the physical nature of the porosity-induced fatigue failure of nickel-base single crystals.

(4) The practicality of the proposed model lies in that only more than three fatigue data are necessary to obtain the S-N curve, though more data are recommended to obtain a higher accuracy.


## ACKNOWLEDGEMENTS

The National Science and Technology Major Project of China (2017-VI-0003-0073) is acknowledged for supporting the present research work.


## CONFLICT OF INTEREST/COMPETING INTEREST

The authors declare that they have no known competing financial interests or personal relationships that could have appeared to influence the work reported in this paper.

## REFERENCES


1. Atwater MA, Guevara LN, Darling KA, Tschopp MA. Solid State Porous Metal Production: A Review of the Capabilities, Characteristics, and Challenges. Adv Eng Mater. 2018;20(7):1700766. https://doi.org/10.1002/adem.201700766
2. Ruttert B, Meid C, Mujica Roncery L, Lopez-Galilea I, Bartsch M, Theisen W. Effect of porosity and eutectics on the high-temperature low-cycle fatigue performance of a nickel-base single-crystal superalloy. Scripta Mater. 2018;155:139-43. https://doi.org/10.1016/j.scriptamat.2018.06.036
3. Epishin A, Camin B, Hansen L, Heuser M, Lopez-Galilea I, Ruttert B, et al. Refinement and Experimental Validation of a Vacancy Model of Pore

Annihilation in Single-Crystal Nickel-Base Superalloys during Hot Isostatic Pressing. Adv Eng Mater. 2021;23(7):2100211.
https://doi.org/10.1002/adem.202100211

4. Logunov AV, Zavodov SA, and Danilov DV. The Challenges in Development of Nickel-Based Heat-Resistant Superalloys for Gas Turbine Disks and Creation of a New Superalloy with Increased Operational Characteristics. Mater Today. 2019;11:459-64.
https://doi.org/10.1016/j.matpr.2019.01.013

5. Shi D, Song J, Qi H, Li S, and Yang X. Effect of interface diffusion on low-cycle fatigue behaviors of MCrAlY coated single crystal superalloys. Int J Fatigue. 2020;137:105660.
https://doi.org/10.1016/j.ijfatigue.2020.105660

6. Bouchenot T, Gordon AP, Shinde S, Gravett P. An Analytical Stress-Strain Hysteresis Model for a Directionally-Solidified Superalloy Under Thermomechanical Fatigue. 2014.
https://doi.org/10.1115/GT2014-27329

7. Rai RK, Sahu JK, Das SK, Paulose N, Fernando DC, Srivastava C. Cyclic plastic deformation behaviour of a directionally solidified nickel base superalloy at 850 °C: Damage micromechanisms. Mater Charact. 2018;141:120-8.
https://doi.org/10.1016/j.matchar.2018.04.039

8. Shi Z, Wang X, Liu S, Li J. Low cycle fatigue properties and microstructure evolution at 760°C of a single crystal superalloy. Prog Nat Sci- Mater Inter. 2015;25(1):78-83.
https://doi.org/10.1016/j.pnsc.2015.01.009

9. Chen G, Zhang Y, Xu DK, Lin YC, Chen X. Low cycle fatigue and creep-fatigue interaction behavior of nickel-base superalloy GH4169 at elevated temperature of 650°C. Mater Sci Eng A. 2016;655:175-82.
https://doi.org/10.1016/j.msea.2015.12.096

10. Zhang L, Zhao LG, Roy A, Silberschmidt VV, McColvin G. Low-cycle fatigue

of single crystal nickel-based superalloy – mechanical testing and TEM characterisation. Mater Sci Eng A. 2019;744:538-47.
https://doi.org/10.1016/j.msea.2018.12.084

11. Liu L, Meng J, Liu J, Zhang H, Sun X, Zhou Y. Investigation on low cycle fatigue behaviors of the [001] and [011] oriental single crystal superalloy at 760 °C. Mater Sci Eng A. 2018;734:1-6.
https://doi.org/10.1016/j.msea.2018.07.078

12. Zhang X, Gao H, Wen Z, Zhang H, Yue Z. Low Cycle Fatigue Failure Analysis of a Ni-Based Single Crystal Superalloys at 850 °C. Adv Eng Mater. 2019;21(2):1800647.
https://doi.org/10.1002/adem.201800647

13. Kashinga RJ, Zhao LG, Silberschmidt VV, Farukh F, Barnard NC, Whittaker MT, et al. Low cycle fatigue of a directionally solidified nickel-based superalloy: Testing, characterisation and modelling. Mater Sci Eng A. 2017;708:503-13.
https://doi.org/10.1016/j.msea.2017.10.024

14. Zhang L, Zhao L, Jiang R, Bullough C. Crystal plasticity finite-element modelling of cyclic deformation and crack initiation in a nickel-based single-crystal superalloy under low-cycle fatigue. Fatigue Fract Eng Mater Struct. 2020:1-15.
https://doi.org/10.1111/ffe.13228

15. Li Z, Wen Z, Gao H, Wu Y. Investigation on low cycle fatigue of nickel‐based single crystal turbine blade in different regions. Materialwiss Werkst. 2018;49(10):1193-205.

16. Ravi Chandran KS. A constitutive equation for the S–N fatigue behavior of metal single crystals and validation by the physical definition of fatigue endurance limit. Int J Fatigue. 2016;91:21-8.
https://doi.org/10.1016/j.ijfatigue.2016.05.020

17. Chandran KSR. A physical model and constitutive equations for complete characterization of S-N fatigue behavior of metals. Acta Mater. 2016;121:85-103.

https://doi.org/10.1016/j.actamat.2016.09.001

18. Vacchieri E, Gallo BG, Guarnone P, Poggio E, Villari P, Holdsworth SR. Safe life approach considering creep-fatigue interaction and Weibull statistics for crack growth evaluation based on field feedback applied to a GT first stage blade. Procedia Structural Integrity. 2017;7:182-9.
https://doi.org/10.1016/j.prostr.2017.11.076

19. Dabiri M, Lindroos M, Andersson T, Afkhami S, Laukkanen A, Björk T. Utilizing the theory of critical distances in conjunction with crystal plasticity for low-cycle notch fatigue analysis of S960 MC high-strength steel. Int J Fatigue. 2018;117:257-73.
https://doi.org/10.1016/j.ijfatigue.2018.07.042

20. Bourbita F, Rémy L. A combined critical distance and energy density model to predict high temperature fatigue life in notched single crystal superalloy members. Int J Fatigue. 2016;84:17-27.
https://doi.org/10.1016/j.ijfatigue.2015.11.007

21. Sun J, Yang S, Yuan H. Assessment of thermo-mechanical fatigue in a nickel-based single-crystal superalloy CMSX-4 accounting for temperature gradient effects. Mater Sci Eng A. 2021;809:140918.
https://doi.org/10.1016/j.msea.2021.140918

22. Zhai Y, Khan MK, Correia J, de Jesus AMP, Huang Z, Zhang X, et al. Effect of secondary crystal orientations on the deformation anisotropy for nickel-based single-crystal plate with notch feature. J Strain Anal Eng. 2019;54(1):54-64.
https://doi.org/10.1177/0309324718819298

23. He X, Zhang Y, Shi H, Gu J, Li C, Kadau K, et al. Influence of orientation and temperature on the fatigue crack growth of a nickel-based directionally solidified superalloy. Mater Sci Eng A. 2014;618:153-60.
https://doi.org/10.1016/j.msea.2014.09.007

24. Segersäll M, Leidermark D, Moverare JJ. Influence of crystal orientation on the thermomechanical fatigue behaviour in a single-crystal superalloy. Mater Sci Eng A. 2015;623:68-77.

25. Kunz L, Horník V, Hutař P, Fintová S. Initiation of fatigue cracks and lifetime of Ni-base superalloys at high mean stress and temperature. Procedia Structural Integrity. 2017;7:44-9.
https://doi.org/10.1016/j.prostr.2017.11.059

26. Segersäll M, Deng D. A comparative study between in- and out-of-phase thermomechanical fatigue behaviour of a single-crystal superalloy. Int J Fatigue. 2021;146:106162.
https://doi.org/10.1016/j.ijfatigue.2021.106162

27. Kanda M, Sakane M, Ohnami M, Hasebe T. High Temperature Multiaxial Low Cycle Fatigue of CMSX-2 NI-Base Single Crystal Superalloy. J Eng Mater T. 1997;119(2):153-60.
https://doi.org/10.1115/1.2805988

28. Sakane M, Isobe N. Tension–torsion multiaxial creep–fatigue lives of the Nickel-based superalloy Alloy 738LC. Int J Fatigue. 2022;155:106575.
https://doi.org/10.1016/j.ijfatigue.2021.106575

29. Tridello A, Niutta CB, Berto F, Paolino DS. Size-effect in Very High Cycle Fatigue: A review. Int J Fatigue. 2021;153:106462.
https://doi.org/10.1016/j.ijfatigue.2021.106462

30. Prithivirajan V, Sangid MD. The role of defects and critical pore size analysis in the fatigue response of additively manufactured IN718 via crystal plasticity. Mater Design. 2018;150:139-53.
https://doi.org/10.1016/j.matdes.2018.04.022

31. Rémy L, Geuffrard M, Alam A, Köster A, Fleury E. Effects of microstructure in high temperature fatigue: Lifetime to crack initiation of a single crystal superalloy in high temperature low cycle fatigue. Int J Fatigue. 2013;57:37-49.
https://doi.org/10.1016/j.ijfatigue.2012.10.013

32. Musinski WD, McDowell DL. Microstructure-sensitive probabilistic modeling of HCF crack initiation and early crack growth in Ni-base superalloy IN100 notched components. Int J Fatigue. 2012;37:41-53.
https://doi.org/10.1016/j.ijfatigue.2011.09.014

33. Cruzado A, Lucarini S, Llorca J, Segurado J. Microstructure-based fatigue life model of metallic alloys with bilinear Coffin-Manson behavior. Int J Fatigue. 2018;107:40-8.
https://doi.org/10.1016/j.ijfatigue.2017.10.014

34. Wan VVC, Jiang J, MacLachlan DW, Dunne FPE. Microstructure-sensitive fatigue crack nucleation in a polycrystalline Ni superalloy. Int J Fatigue. 2016;90:181-90.
https://doi.org/10.1016/j.ijfatigue.2016.04.013

35. Briffod F, Shiraiwa T, Enoki M. Microstructure modeling and crystal plasticity simulations for the evaluation of fatigue crack initiation in α-iron specimen including an elliptic defect. Mater Sci Eng A. 2017;695:165-77.
https://doi.org/10.1016/j.msea.2017.04.030

36. Chen B, Jiang J, Dunne FPE. Microstructurally-sensitive fatigue crack nucleation in Ni-based single and oligo crystals. J Mech Phys Solids. 2017;106:15-33.
https://doi.org/10.1016/j.jmps.2017.05.012

37. Salajegheh N, McDowell DL. Microstructure-sensitive weighted probability approach for modeling surface to bulk transition of high cycle fatigue failures dominated by primary inclusions. Int J Fatigue. 2014;59:188-99.
https://doi.org/10.1016/j.ijfatigue.2013.08.025

38. Przybyla CP, Musinski WD, Castelluccio GM, McDowell DL. Microstructure-sensitive HCF and VHCF simulations. Int J Fatigue. 2013;57:9-27.
https://doi.org/10.1016/j.ijfatigue.2012.09.014

39. Murakami Y. Metal fatigue: effects of small defects and nonmetallic inclusions. Academic Press; 2019.

40. Li P, Yao W, Shi H, Luo P, Hua Y. A topologized resolved shear stress method for the life prediction of nickel-base single crystal superalloys. Theor Appl Fract Mech. 2020;108:102624.
https://doi.org/10.1016/j.tafmec.2020.102624

41. Jiang W, Yao W, Li P, Luo P. A fatigue life prediction method distinguishing

fracture modes for Ni-based single crystal superalloys considering porosity defect. Theor Appl Fract Mech. 2020:102883.
https://doi.org/10.1016/j.tafmec.2020.102883

42. Li P, Yao W, Jiang W. Orientation-dependent low cycle fatigue performance of Nickel-base single crystal superalloy at intermediate temperature range. Mater Today Commu. 2021;26:101836.
https://doi.org/10.1016/j.mtcomm.2020.101836

43. Jiang W, Li P, Yao W-X, Rui S-S, Shi H-J, Huang J. The effect of porosity size on the high cycle fatigue life of nickel-based single crystal superalloy at 980°C. Int J Fatigue. 2021;147:106191.
https://doi.org/10.1016/j.ijfatigue.2021.106191

44. Murakami Y. Material defects as the basis of fatigue design. Int J Fatigue. 2012;41:2-10.
https://doi.org/10.1016/j.ijfatigue.2011.12.001

45. Nicoletto G, Konečná R, Fintova S. Characterization of microshrinkage casting defects of Al–Si alloys by X-ray computed tomography and metallography. Int J Fatigue. 2012;41:39-46.

46. Bortoluci Ormastroni LM, Mataveli Suave L, Cervellon A, Villechaise P, Cormier J. LCF, HCF and VHCF life sensitivity to solution heat treatment of a third-generation Ni-based single crystal superalloy. Int J Fatigue. 2020;130:105247.
https://doi.org/10.1016/j.ijfatigue.2019.105247

47. Jiang W, Li P, Yao W-X, Rui S-S, Shi H-J, Huang J. The effect of porosity size and oxidation on the HCF property of nickel-based single crystal superalloy at 980 ℃. Theor Appl Fract Mech. 2022;120:103423.
https://doi.org/10.1016/j.tafmec.2022.103423